Earthquake Engineering, Tenth World Conference © 1992 Balkema, Rotterdam. ISBN 90 5410 060 5

Very low-cycle fatigue tests of steel angle members under earthquake loading

Satoshi Iwai, Yeon-Soo Park, Taijiro Nonaka & Hiroyuki Kameda
Disaster Prevention Research Institute, Kyoto University, Japan

ABSTRACT: An experimental investigation has been performed on very low-cycle fatigue of steel angle members under large repeated deformations. The angle specimen was subjected to repeated axial load after undergoing inelastic buckling. The objective of this study is to extract decisive factors causing cracks and rupture in the course of loading repetitions of the order of a few to twenty cycles. The experimental results show that energy dissipation capacities depend heavily on the entire history of loading, failure modes, slenderness ratios and width-to-thickness ratios. No simple quantitative relations were observed between initiation of visible cracks and the energy dissipation capacity. Visible cracks were located near the regions of severe concentration of strains. The maximum values of residual "net" strains, excluding contributions from the crack opening, of all the specimens are of the order of 25-40% and they do not depend on loading patterns, failure modes, slenderness ratios and width-to-thickness ratios.

1 INTRODUCTION

Well-designed steel structures are expected to undergo partial plastic deformation under strong seismic excitations. Structural damage and failure are often associated with plastic and/or unstable behavior of structural members due to large cyclic deformations with initiation of local buckling. Therefore, it is important to identify the decisive factors causing failure due to very low cycles of loading, which is herein meant to be structural fatigue under load repetitions of the order of a few to twenty cycles. Previous experimental research on very low-cycle fatigue had been done for thin-plate elements in a steel member (Iwai et al. 1990). The research result showed that the state of ultimate failure under cyclic loading is strongly related to the maximum residual strain taking place at an edge in the cross section. The study in this paper is focused on extracting decisive factors causing cracks and rupture in the inelastic post-buckling behavior of steel members, and on clarifying the quantitative relationships among the important physical factors causing failure. Particular attention is paid to the effects of loading patterns, failure modes and cross sectional shapes on very low-cycle fatigue behavior.

Table 1. Mechanical properties of materials.

Type	Angle	Yield stress (N/mm^2)	Ultimate strength (N/mm^2)	Elongation (%)
I	L-40x40x3	371	465	31.2
II	L-40x40x3	336	449	29.7
III	L-40x40x5	339	469	27.1

2 TEST PROGRAM

The test specimens were angles L-40x40x3 and L-40x40x5 of SS41 grade. The yield stress σ_y and the ultimate tensile strength of the materials are shown in Table 1. A total of 20 specimens was tested. Each specimen was pin-supported at each end by holding a steel plate, which was attached through welds perpendicularly to the specimen, as indicated in Fig. 1. The specimen had the effective length l of the tested part between the pin-supports being 318mm (or 300mm) or 618mm, as shown in Fig. 2 and Table 2. The experiments were performed up to occurrence of visible cracks or rupture of the specimen, in order to observe the deteriorating process and the state of cumulative plastic strains at the critical part of the specimen. Test parameters are summarized as follows;

(1) slenderness ratio $\lambda = l/i$
(where i is the radius of gyration with respect to the v axis of the cross section in Fig. 1(d))
(2) width-to-thickness ratio b/t
(3) loading pattern
(4) deflection mode.

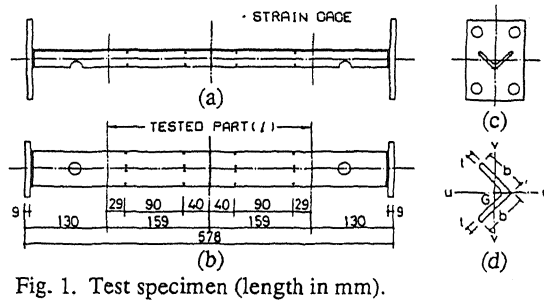

Fig. 1. Test specimen (length in mm).

The λ value of the specimens ranged 37-41 and 77. The value of b/t was selected 14.0-16.4 and 8.6, as shown in Table 2. The choices of (3) were from increased displacement amplitude (I type) loading, constant displacement amplitude (C type) loading, and stepwise displacement amplitude (G and S types) loading, in the contraction side of the relative axial displacement Δ, as shown in Fig. 3. The total numbers of load cycles were set in the loading program up to 24 and 30 in the I type and the C, G, S types, respectively. The definition of (4) is described in section 3.1.

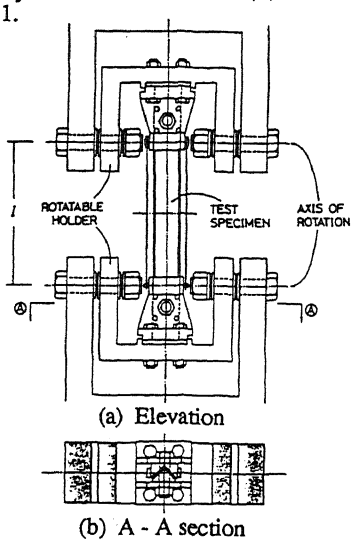

(a) Elevation

(b) A - A section

Fig. 2. Specimen supporting system.

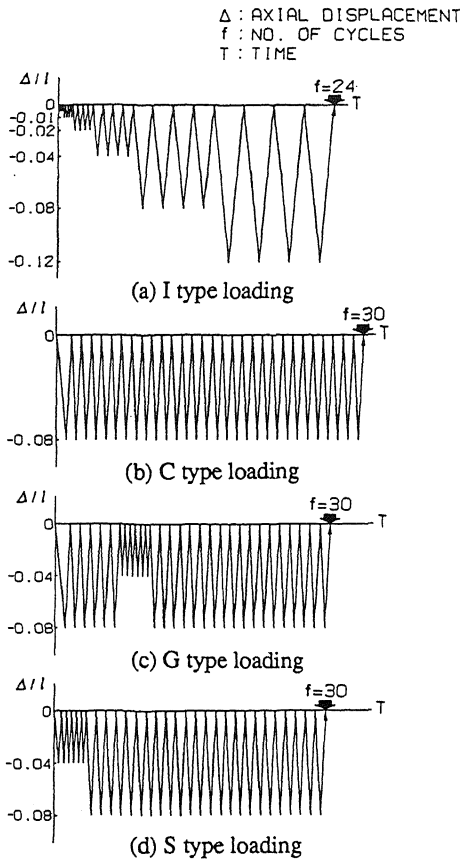

Fig. 3. Loading patterns.

Table 2. Specimen sizes and test parameters.

Specimen Name	No.	Material type	Length l (mm)	Width b (mm)	Thickness t (mm)	Slenderness ratio λ	Width-to-thickness ratio b/t	Loading pattern	Deflection mode
L3IP	13	I	318	39.6	2.80	40.5	14.1	I	P
L3IN	4	II	301	40.4	2.55	37.4	15.8	I	N
$L3CP_a$	6	II	300	40.3	2.55	37.3	15.8	C	P
$L3CP_b$	18	I	318	39.6	2.83	40.5	14.0	C	P
L3CN	5	II	301	40.5	2.47	37.4	16.4	C	N
L3GP	16	I	318	39.5	2.80	40.5	14.1	G	P
L3SP	17	I	318	39.5	2.82	40.5	14.0	S	P
L3GN	14	I	318	39.5	2.78	40.5	14.2	G	N
L3SN	15	I	318	39.6	2.79	40.5	14.2	S	N
L5IP	9	III	318	39.2	4.56	41.4	8.6	I	P
L5IN	7	III	300	39.2	4.58	39.0	8.6	I	N
$L5CP_a$	8	III	317	39.3	4.55	41.2	8.6	C	P
$L5CP_b$	10	III	317	39.2	4.55	41.2	8.6	C	P
L5CN	11	III	318	39.2	4.55	41.4	8.6	C	N
H3IP	19	II	618	40.3	2.49	76.8	16.2	I	P
H3IN	21	II	618	40.2	2.50	76.8	16.1	I	N
H3CP	20	II	618	40.3	2.50	76.8	16.1	C	P
H3CN	22	II	618	40.4	2.50	76.8	16.2	C	N
H3GP	23	II	618	40.2	2.51	76.8	16.0	G	P
H3SP	24	II	618	40.4	2.49	76.8	16.2	S	P

A slowly varying uni-axial load was applied to near-centroid G of the cross section of the specimen (see Fig. 1(d)), using a hydraulic servo actuator with a loading capacity of 294kN. A very small eccentricity for load (about ±0.5mm in the u-direction) was given to control the deflection mode. Loading was controlled by the relative axial displacement Δ, programmed as in Fig. 3, between both ends approaching each other. This causes buckling in the specimen under first compressive loading, and induces very large strains. In order to measure residual local strains after testing, dots were marked on the surface at the both edges and the corner in the cross section, in the direction parallel to the longitudinal axis at intervals of 2mm for a mid-part length of 80mm, using a Vickers hardness tester.

3 TEST RESULTS

3.1 *Buckling and cracking behavior*

Fig. 4 is a sketch of the buckling deformation and the states of visible cracking. The positive (P type) and negative (N type) deflection modes were observed as defined in the figure. The global buckling deformation was accompanied by large deformation due to local buckling of the plates of the leg at the mid-part of the specimen. Fig. 5 shows the observed compressive strength in relation to the column curve, where σ_{cr} is the buckling stress and E_s the Young's modulus.

Typical examples of the load-axial displacement relationships of the specimens are shown in Fig. 6.

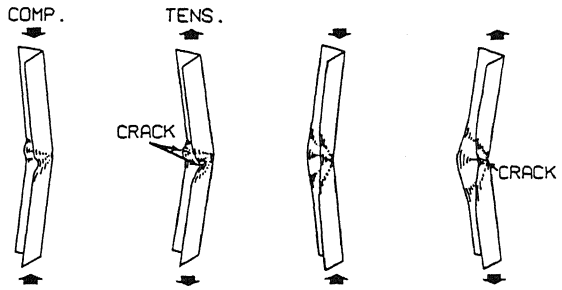

(a) Positive deflection mode (b) Negative deflection mode

Fig. 4. Deflection modes and cracking patterns.

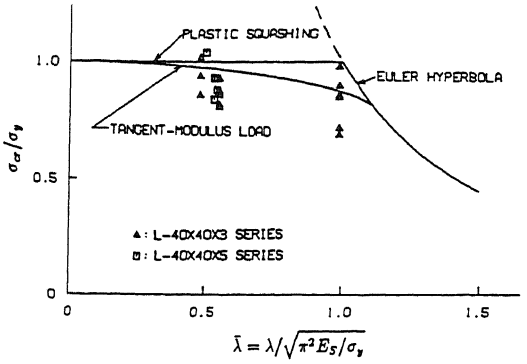

Fig. 5. Column curve and observed strength.

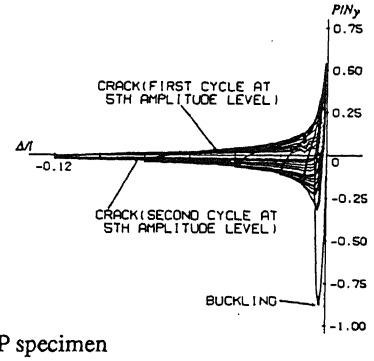

(a) L3IP specimen

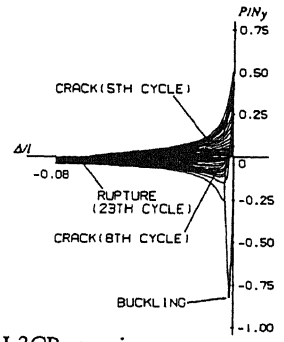

(b) L3CP$_b$ specimen

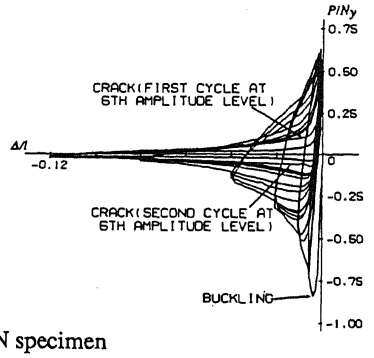

(c) L3IN specimen

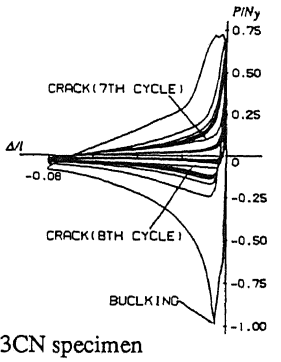

(d) L3CN specimen

Fig. 6. Load-axial displacement relations.

Here the load P and relative displacement Δ are normalized by the yield load N_y and length l, respectively, and are given as positive for tension. Numbers of load cycles at three cracking states and rupture are shown for each specimen in Table 3. Irrespective of the loading patterns and deflection modes, visible cracks were initiated during stretching on the concave side of the overall buckling deformation (f_{cav}) induced in the preceding load cycles. Visible cracks at the convex side (f_{vex}) were observed within 1-3 cycles following the concave side cracking. Cracking at the concave and convex sides rapidly penetrated through the thickness of the legs (f_{pen}).

In most specimens subjected to the I type loading, no cracks were observed under the repetition of global strain Δ/l smaller than 8%, but visible cracks were initiated in the 1st cycle at the amplitude level of 12% global strain. In the cases of the C type loading under 8% global strain, visible cracks occurred during the 5-9th cycle. Inelastic buckling caused a sudden decrease in the compressive load-carrying capacity, but only a slight decrease in the succeeding tensile load-carrying capacity. However, both the compressive and tensile load-carrying capacities were considerably decreased by the initiation of cracking (see Fig. 6). It is thus found that the ultimate stage of failure is closely related to the occurrence of a visible crack. The cracks were quickly enlarged in the course of load repetitions. Nine specimens, for which the value f_{rup} is indicated in Table 3, were completely ruptured within the programmed loading cycles. The test results show that f_{rup} decreases as b/t becomes smaller and λ becomes larger. This may be because the local deformation of the angle was severely concentrated in these cases.

The specimens $L3CP_a$, $L3CP_b$, $L5CP_a$ and $L5CP_b$ were subjected to the same loading condition. The latter two of identical angles showed very similar load-displacement curves and completely ruptured in the identical 19th cycle, indicating the trustworthiness of this series of test.

3.2 *Energy dissipation behavior*

Dissipated energy was calculated by the summation of the areas surrounded by the load-axial displacement curves. The relationships between the dissipated energy E and the number of cycles f are shown in Fig. 7 for all the specimens, where $E_o = \sigma_y^2 Al / (2E_s)$ (in which A is cross sectional area) is the maximum elastic strain energy which can be stored in the tested part of the specimen. In the cases of the same loading pattern and the same deflection mode, very similar processes of energy dissipation were observed (see curves for $L5CP_a$ and $L5CP_b$, and $L3CP_a$ and $L3CP_b$ in Fig. 7(b)). However, if deflection modes are different, cumulative energy dissipation behavior is quite different even among specimens under the same loading pattern (see Figs. 7(a) and (b)); the P-Δ curves in the case of the positive deflection mode show thinner hysteresis loops than the negative deflection mode (compare (a) with (c), and (b) with (d) in Fig. 6). Energy dissipation capacitiy is seen to be affected by the deflection mode.

From comparison of three types of loading patterns, C, G and S, effects of loading sequence are investigated. In the case of the positive deflection

Table 3. Test results.

Specimen Name	Buckling load P_{cr} (kN)	Number of load cycles: Crack f_{cav}	Crack f_{vex}	Crack f_{pen}	Rupture f_{rup}	Dissipated energy E/E_o	Strain at cracked portion: Tens. ε_{tens} (%)	Comp. ε_{comp} (%)
L3IP	70.6	17	18	18	--	131	--	--
L3IN	58.0	20	21	21	--	235	--	--
$L3CP_a$	62.9	9	10	10	--	133	27.5	-29
$L3CP_b$	66.1	5	8	8	23	115	30	-32.5
L3CN	68.3	7	8	8	--	220	--	-41
L3GP	64.9	5	9	10	25	112	27.5	-35
L3SP	68.7	8	12	12	27	122	30	-32.5
L3GN	70.1	6	--	7	--	170	--	-30
L3SN	74.4	10	--	11	--	221	--	-35
L5IP	100.7	21	23	23	--	236	35	-35
L5IN	119.1	22	--	22	--	410	--	-30
$L5CP_a$	95.6	9	12	12	19	211	32.5	-35
$L5CP_b$	106.3	9	12	12	19	214	30	-32.5
L5CN	106.5	9	13	13	21	378	35	-35
H3IP	65.9	18	21	21	--	78	35	-35
H3IN	56.7	18	--	22	--	117	--	-35
H3CP	48.6	5	8	9	17	66	32.5	-35
H3CN	57.6	5	--	8	--	104	--	-35
H3GP	46.1	6	9	11	22	75	30	-35
H3SP	60.5	9	12	12	22	83	35	-35

mode (see Figs. 7(c) and (e)), the number of cycles at rupture f_{rup} is small in the order of the C, G and S types of loading. But the energy dissipation capacity is not significantly different among these three types.

No simple quantitative relations were observed between the initiation of a visible crack or the rupture of a specimen and the energy dissipation capacity. Energy dissipation process and capacity depend on the entire history of loading, deflection modes, slenderness ratios and width-to-thickness ratios.

3.3 *Local strain distributions*

Fig. 8 shows typical distributions of residual local strains accumulated at the edges and corners in the cross sections after testing. Visible cracks are located near the regions of severe concentration of strains. The maximum absolute values of residual "net" strains, excluding contributions from the crack opening, of all the specimens were in the range of 25-35% on the elongation side and 30-40% on the contraction side (see ε_{tens} and ε_{comp} in Table 3), and they do not depend on loading patterns, deflection modes, slenderness ratios and width-to-thickness ratios. For comparison, Fig. 9 shows the local strain distributions in the monotonic tensile test of a JIS (Japanese Industrial Standard) 13-B type specimen. The maximum net strain at ruptured portion, measured at 1.5mm or 2mm intervals, in this material test was about 100%, even though the average elongation was about 30%. The residual strain values in the angle tests reflect the effects of repeated loading. Analytical study is under way by means of numerical simulation in relation to these phenomena.

4 CONCLUSIONS

The main conclusions from this investigation are summarized as follows:

1. The experimental investigation reveals that, regardless of loading patterns and deflection modes, visible cracks were initiated during stretching on the concave side of the overall bending deformation induced in the preceding load cycles.

2. The number of load cycles at rupture decreases as width-to-thickness ratio becomes smaller and slenderness ratio becomes larger, because of severe concentration of local deformation in angles.

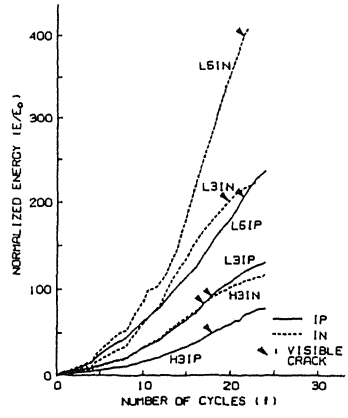

(a) I type loading

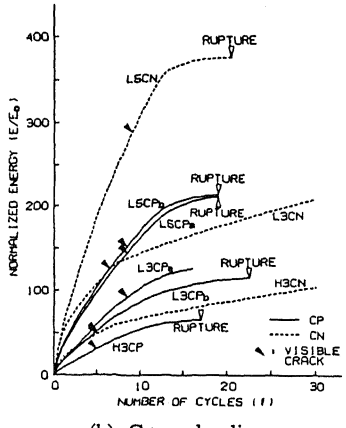

(b) C type loading

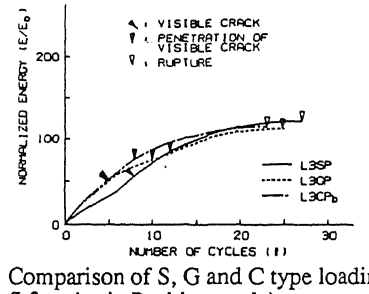

(c) Comparison of S, G and C type loading (L3 series in Positive mode)

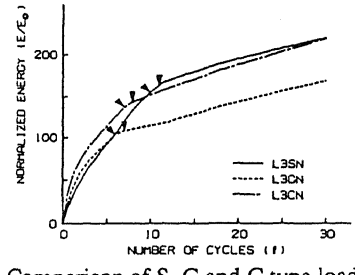

(d) Comparison of S, G and C type loading (L3 series in Negative mode)

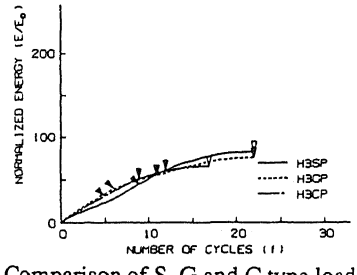

(e) Comparison of S, G and C type loading (H3 series in Positive mode)

Fig. 7. Comparison of energy dissipation in the course of increasing number of cycles.

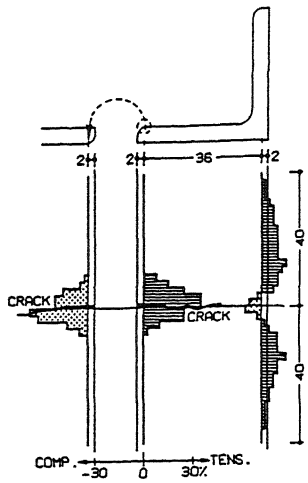

(a) Positive deflection mode (L5IP)

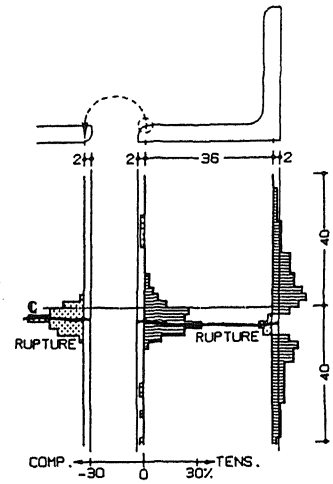

(b) Positive deflection mode ($L5CP_a$)

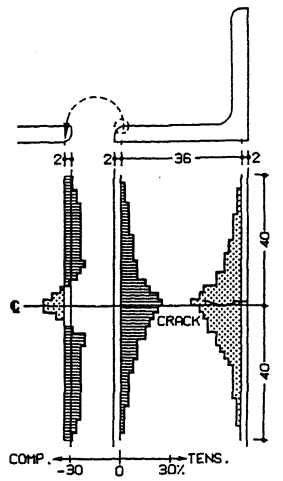

(c) Negative deflection mode (L5IN)

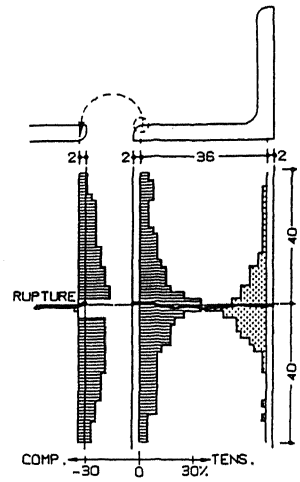

(d) Negative deflection mode (L5CN)

Fig. 8. Distribution of local strain in angle test.

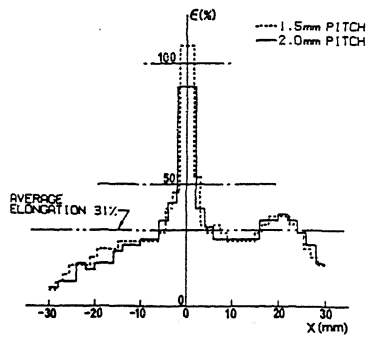

Fig. 9. Distribution of local strain in material test.

3. The reappearance of very low-cycle fatigue behavior was observed under the identical loading pattern and deflection mode, indicating the trustworthiness of this experimental investigation.

4. Energy dissipation capacity depends heavily on the entire history of loading, failure mode, slenderness ratio and width-to-thickness ratio.

5. Residual strains at the outbreak of a visible crack under very low-cycles of loading were of the order of 25-40%, regardless of the loading patterns, deflection modes, slenderness ratios and width-to-thickness ratios.

REFERENCE

Iwai, S., T. Nonaka, U. Bourgund and H. Kameda, 1990. Structural Failure due to Very Low cycle Fatigue of Steel Members and Elements under Earthquake Loading, *Proc. of 8th Japan Earthquake Engineering Symposium*, Vol. 2, pp. 1377-1382.